Coherence and Transients in Nonlocally Coupled Dissipative Kicked Rotors

Jin Yan[1, *]

[1] *Weierstrass Institute for Applied Analysis and Stochastics, Mohrenstraße 39, 10117 Berlin, Germany*

The dynamics of nonlocally coupled dissipative kicked rotors is rich and complex. In this study, we consider a network of rotors where each interacts equally with a certain range of its neighbors. We focus on the influence of the coupling strength and the coupling range, and show both analytically and numerically the critical transitions in the phase diagram, which include bifurcations of simple spatiotemporal patterns and changes in basin sizes of coherent states with different wavenumbers. We highlight that this diagram is fundamentally different from those found in other coupled systems such as in coupled logistic maps or Lorenz systems. Finally, we show an interesting domain-wall phenomenon in the coupled chaotic rotors, where a super-long transient interface state (partially regular and partially chaotic) is observed and can persist exponentially long as the coupling range increases up to a critical threshold.

I. INTRODUCTION

The emergence of synchronized and correlated dynamics among coupled elements are fundamental phenomena observed in a wide range of complex systems, from biological neural networks to laser arrays and chemical oscillators. These behaviors typically emerge from the interplay between interactions and intrinsic properties [1]. Beyond full synchronization, a variety of structured yet non-chaotic states, such as phase-locking [2], metastability [3, 4], cluster formation [5] and partial synchronization [6, 7], illustrate how systems can transiently coordinate while retaining diverse localized activities.

In many real-world settings, interactions are neither purely nearest-neighbor (local) nor all-to-all (global, where every element interacts equally with all others), but extending over finite spatial ranges, leading to nonlocal couplings. Such couplings give rise to rich spatiotemporal patterns that are often absent in local or global cases. One of the most well-known examples is chimera states, characterized by the coexistence of coherent and incoherent domains [8, 9]. The interplay between the coupling range and strength makes the transition between order and disorder more intricate and complex [10, 11].

However, the analysis of nonlocal coupling presents significant theoretical challenges, as it eludes the simplifying symmetries of all-to-all coupling via mean-field approaches (e.g., the Kuramoto model reduces to a single order parameter), and the spatial regularity of nearest-neighbor coupling via reaction-diffusion PDEs or discrete Laplacians. Nonlocal systems, with their distance-dependent interactions – require more sophisticated approaches. The seminal work [11] demonstrated this through coherence-incoherence transitions in nonlocally coupled logistic maps, and confirmed that such a transition is universal among systems with diverse local dynamics. Inspired by this, we present an analytical and numerical study of various transitions in a nonlocally coupled system with a two-dimensional local map, specifically the dissipative kicked rotor [12–14]. Interestingly, despite the nonlocal coupling, linear stability analysis effectively captures the dynamics of the coupled system beyond the linearization regime; the resulting phase diagram exhibits qualitatively different structure compared to previously studied systems [11]. Analyzing bifurcations of simple states reveals transition points between coherent states of different spatial periodicity, and between coherent and incoherent states. These will be illustrated in detail.

The second part of our work investigates super-long transients in systems where the local map has both non-chaotic and chaotic attractors. This regime is generic and intermediate between regular and fully chaotic behavior. When initialized with a cluster-like configuration, the system eventually evolves toward a fully chaotic state; however, the lifetime of a cluster-like state can be exponentially long depending on the coupling range. Remarkably, beyond a critical point, a sudden transition occurs, causing the transient lifetime to collapse by several orders of magnitude. The significance of these findings lies in the observation that cluster-like states are often desirable in real-world applications. Such states can support structured behavior or partial predictability and thus useful in neuroscience, power grids and information processing [15–18]. Alternatively, in other contexts, a rapid onset of full chaos may be desirable [17–20]. By tuning the coupling parameters, it becomes possible to sustain such states for a controllably long duration, offering a practical mechanism to delay the onset of full chaos, or to reduce transient time by adding more connections to the system.

The paper is organized as follows. In Sec.II we introduce the model and parameters. In Sec.III we study analytically the transition from a homogeneous state to a temporal period-2 state with a characteristic wavenumber, and identify the phase transitions under variations of the coupling length and strength. These are supported by numerical simulations. In Sec.IV we explore transient behavior when local rotors have a dominant chaotic attractor. We give a heuristic understanding of the super-long transient time.

* jin.yan@wias-berlin.de

II. MODEL

We consider a chain of N nonlocally coupled dissipative kicked rotors with periodic boundary conditions, described by

$$\begin{aligned} p_j(t+1) =&\gamma p_j(t) - K_0 \sin\theta_j(t) \\ &+ \frac{K}{2P_c}\sum_{k=j-P_c}^{j+P_c} \sin(\theta_k(t)-\theta_j(t)) \qquad (1) \\ \theta_j(t+1) =&\theta_j(t) + p_j(t+1) \pmod{2\pi} \end{aligned}$$

where $(p_j(t), \theta_j(t)) \in (-\infty, +\infty)\times[0, 2\pi)$ denote the momentum and angle of the rotor $j \in \{1, 2, ...N\}$ at time $t \in \mathbb{N}_0$, $\gamma \in (0, 1)$ is the dissipation coefficient, $K_0 > 0$ is the local nonlinearity parameter, $K > 0$ is the coupling strength, and $P_c \in \left\{1, 2, .., \frac{N}{2}\right\}$ (assuming N is even) is the coupling length, denoting the number of neighbors in each direction that are coupled to the rotor j.

The local map describes a dissipative kicked rotor and for a fixed γ the system undergoes multiple bifurcations under variations of K_0 [14]. For the nearest-neighbor case ($P_c = 1$), see [14].

In this paper, we fix $\gamma = 0.8$ without loss of generality [14], use $K_0 = 2$ (local map is non-chaotic and has three fixed points as the only attractors) for Sec.III, and use $K_0 = 6.6$ (local map has coexisting non-chaotic and chaotic attractors) for Sec.IV. Our focus is on the dynamics arising from the interplay between the coupling strength K and the coupling length P_c.

III. SPATIAL AND TEMPORAL PATTERNS

In this section, we focus on the following three issues. The first one is the transition from the stationary, fully synchronized state to a coherent state of temporal period-2, which can be explained analytically through a linear stability analysis. A wavenumber will be defined to characterize the spatial periodicity. The second issue is to study coherent regions on the parameter (P_c, K)-plane, particularly the regions with low spatial and temporal periods. The transition curves can be obtained from stability analysis of the temporal period-2 states. The third issue concerns the coexistence of the temporal period-2 states with different wavenumbers, and we numerically examine how their relative basin sizes vary with the coupling length P_c.

Throughout this section, purely random initial conditions are used for numerical simulations: $(p_j(0), \theta_j(0)) \in \mathrm{Uni}[-p_0, p_0] \times \mathrm{Uni}[0, 2\pi)$, where $p_0 > 2\pi$ is constant (the specific value of p_0 does not influence the qualitative results).

A. Transition from zero homogeneous states

The full phase space of the system (1) is a product of N infinite cylinders $(p_j, \theta_j) \in (-\infty, +\infty) \times [0, 2\pi)$, $\forall j = 1, 2, ..., N$. For K_0 and K both small, trajectories initially close to $\boldsymbol{p} := (p_1, p_2, ..., p_N) = \boldsymbol{0}$ will converge to the *zero synchronized state* $(\boldsymbol{p}, \boldsymbol{\theta}) = (\boldsymbol{0}, \boldsymbol{0})$ and it appears as the only attractor. However, due to multistability of the local map [14], more attractors can be observed when we consider longer truncated cylinders (i.e., $\boldsymbol{p}$ further away from $\boldsymbol{0}$), and the notion of the zero synchronized state is extended to a state in which most rotors are homogeneous but with a few exceptions; these exceptional rotors stay at the nonzero fixed points of the local map. We refer such a state a *zero homogeneous state*. An example is shown in Fig.1(a): for $K_0 = 2$ the local map has three fixed points $p = 0, \pm 2\pi$, where $p = 0$ has the largest basin and $\pm 2\pi$ have equal basin sizes [14].

This kind of zero homogeneous states undergoes a transition to a temporal period-2 state with a spatial periodicity, an example is shown in Fig.1(b). Further increasing the coupling strength K reduces the number of exceptional rotors, leading to a more coherent pattern, cf. Fig.1(c).

This period-doubling bifurcation can be understood analytically via a linear stability analysis. Under the assumption of slow angle variations, the equations of momenta can be linearized as

$$p_j(t+1) = \gamma p_j(t) - K_0\theta_j(t) + \frac{K}{2P_c}\left[\sum_{k=j-P_c}^{j+P_c}\theta_k(t) - 2P_c\theta_j(t)\right].$$

By a Fourier transform $p_j(t) = \sum_w P_w(t)e^{iwj}$, $\theta_j(t) = \sum_w \Theta_w(t)e^{iwj}$, $w = \frac{2\pi l}{N}$, $l = 0, 1, ..., N-1$ (for periodic boundary conditions) we have, for each Fourier mode w,

$$P_w(t+1) = \gamma P_w(t) + \left[-(K_0+K) + \frac{K}{P_c}\sum_{k=1}^{P_c}\cos(wk)\right]\Theta_w(t).$$

The linearized equations of motion thus become

$$\begin{pmatrix} P_w(t+1) \\ \Theta_w(t+1) \end{pmatrix} = \begin{pmatrix} \gamma & A \\ \gamma & 1+A \end{pmatrix}\begin{pmatrix} P_w(t) \\ \Theta_w(t) \end{pmatrix},$$

$$A := -(K_0+K) + \frac{K}{P_c}\sum_{k=1}^{P_c}\cos(wk).$$

The characteristic equation $\lambda^2 - (\gamma+1+A)\lambda + \gamma = 0$ gives the critical behavior at $|\lambda| = 1$. We denote $\lambda_w^\pm := \frac{1}{2}\left[(\gamma+1+A) \pm \sqrt{(\gamma+1+A)^2 - 4\gamma}\right]$. It can be shown that $\max_w |\lambda_w^+| < 1$ for all parameter values under consideration. So the critical point is given by $\max_w |\lambda_w^-| = 1$. Further, the observed period-doubling bifurcation indicates $\min_w \lambda_w^- = -1$, which gives $A = -2(1+\gamma)$. Since $\lambda_w^-(A)$ increases with A, this is achieved at $A = \min_w A$, i.e., $S(w) := \sum_{k=1}^{P_c}\cos(wk) = \csc\frac{w}{2}\sin\frac{P_c w}{2}\cos\frac{(P_c+1)w}{2}$

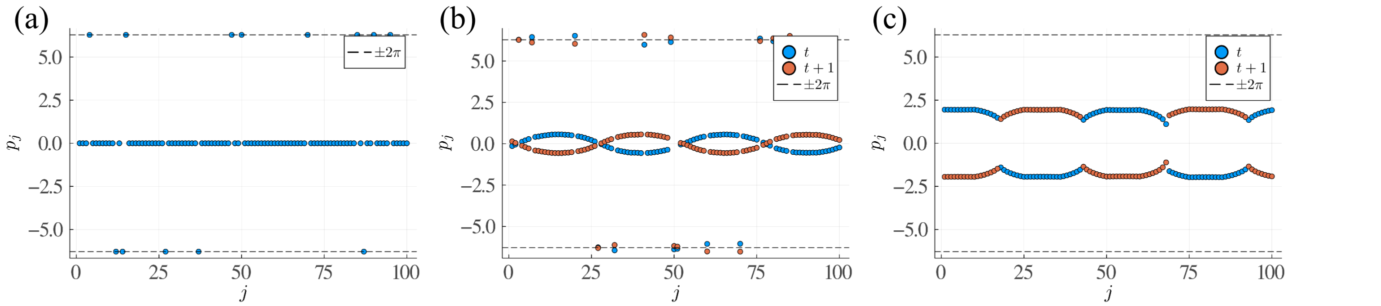

FIG. 1. Snapshots of momenta for (a) $K = 1.3$, (b) $K = 1.4$ and (c) $K = 3$. Other parameters: $\gamma = 0.8$, $K_0 = 2$, $P_c = 32$, $N = 100$ and random initial conditions $(p_j(0), \theta_j(0)) \in \text{Uni}[-35, 35] \times \text{Uni}[0, 2\pi)$, $j = 1, 2, ..., N$. The corresponding angles behave similarly.

is minimized. In terms of the system parameters,

$$K = [2(1+\gamma) - K_0]\frac{P_c}{P_c - S_{\min}},$$
$$S_{\min} := \min_w \left[\csc\frac{w}{2}\sin\frac{P_c w}{2}\cos\frac{(P_c+1)w}{2}\right]. \tag{2}$$

Note that, in the case of nearest-neighbor coupling ($P_c = 1$), $S_{\min} = -1$ at $w = \pi$, and it gives $K_0 = -2K + 2(1+\gamma)$, which is consistent with the result in [14] (where $K \equiv 2J$).

We can infer the spatial period of the temporal period-2 state after the bifurcation. For example, for the patterns illustrated in Fig.1 ($N = 100, P_c = 32$), we have $\tilde{S}_{\min} = \min_w \left[\csc\frac{w}{2}\sin\frac{3w}{2}\cos\frac{33w}{2}\right] \approx -7.56572$ at $\tilde{w} \approx 0.13827$, by $w = \frac{2\pi l}{N}$, we have $\tilde{l} \approx 2.2$. Since the modes w (and l) are discrete, we have denoted the continuous values by tilde. The closest integer is $l = 2$ and the corresponding $S_{\min} \approx -6.94219$. The bifurcation point given by Eq.(2) is therefore $K \approx 1.31$. We refer the spatial period $l = 2$ as the *wavenumber*.

For the system of size $N = 100$ to form a wavenumber $l = 1$, one would require $w = \frac{2\pi}{100}$ and the critical P_c should thus be given by $S_{\min} = S\left(\frac{2\pi}{100}\right)$, which could be achieved only when $P_c = 71 > \frac{N}{2}$. Thus, the lowest realizable wavenumber for the $N = 100$ system is $l = 2$. However, higher wavenumbers are possible: for example, an $l = 3$ pattern emerges at $P_c = 23$, $l = 4$ at $P_c = 17$, $l = 5$ at $P_c = 14$, and so on. Patterns with these wavenumbers are illustrated in Fig.2.

We note here that the wavenumber for the bifurcated state depends on the system size N. For a finite-size system, the eigenvalues $\lambda^-(l)$ are coarse-grained from the continuous ones $\lambda^-(\tilde{l})$, where, a coarser discretization (i.e., smaller N) would result in a less number of unstable eigenmodes. In a continuum limit ($N \to \infty$), the onset of instability occurs earlier than in any finite-size system. It implies that, while a smaller system realizes only one spatial pattern, therefore attracting all initial conditions in the phase space, a larger system can display multistability and realizes spatial patterns with different basin sizes. This will be discussed in the following subsection.

B. Coherent regions and their basin sizes

[11, 21] illustrates a generic phase diagram of spatiotemporal patterns in coupled systems, where a series of decreasing-sized tongue regions highlights the coherent patterns of an increasing wavenumber and (temporal) period-doubling within each tongue. The models studied therein are coupled logistic maps, Lorenz and Rössler systems, and parameters are chosen such that the local dynamics is chaotic. Similar diagrams are also observed in other systems such as Stuart-Landau oscillators [22] and coupled Chebyshev maps (Appendix A). Here, with non-chaotic dissipative kicked rotor maps, we show that the phase diagram is qualitatively different from those in the above mentioned systems. We plot in Fig.3 the diagrams for typical wavenumbers l and temporal periods τ separately.

We describe the different regions by the following five layers on the (P_c, K)-plane, and refer them in Fig.3(b). The layers can be roughly characterized by the range of the coupling strength K:

- Layer-I ($K \lesssim 0.4$): when the coupling is very weak, the zero homogeneous states ($l = 1$, $\tau = 1$) are dominant. This is well-understood from the uncoupled system that the zero fixed point has the largest basin compared to the other fixed points;
- Layer-II ($0.4 \lesssim K \lesssim 1.1$): a type of temporal period-4 states with irregular spatial patterns dominates and coexists with the zero homogeneous states; note that it cannot be a synchronized state (i.e., not a low-dimensional attractor) since otherwise the system would reduce to the local map, where no stable period-4 state exists for $K_0 = 2$;
- Layer-III ($1.1 \lesssim K \lesssim 1.5$): this is a transition regime where a type of temporal period-6 states with irregular spatial patterns dominates, but it appears only for a narrow window of K;
- Layer-IV ($1.5 \lesssim K \lesssim 3.0$): temporal period-2 states with well-defined wavenumbers l are dominant, which is a result from the period-doubling bi-

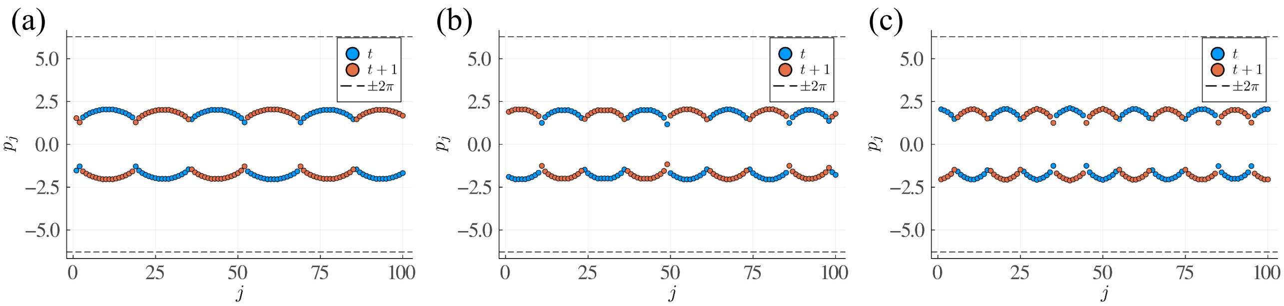

FIG. 2. Snapshots of momenta for (a) $P_c = 23$, (b) $P_c = 17$ and (c) $P_c = 14$. Other parameters: $\gamma = 0.8$, $K_0 = 2$, $K = 3$, $N = 100$ and random initial conditions $(p_j(0), \theta_j(0)) \in \mathrm{Uni}[-35, 35] \times \mathrm{Uni}[0, 2\pi)$, $j = 1, 2, ..., N$. The corresponding angles behave similarly.

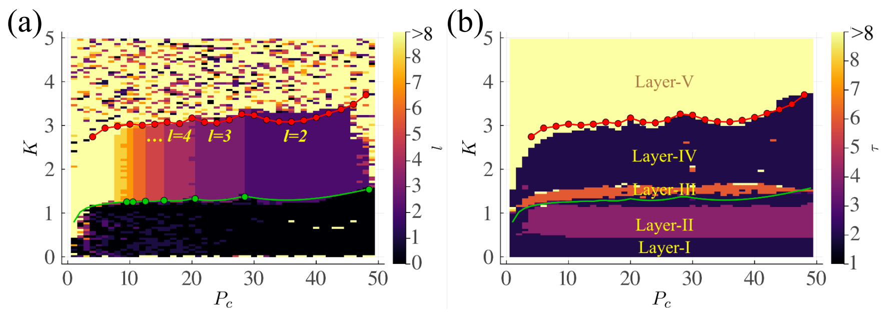

FIG. 3. Regions of (a) wavenumbers $l \leq 8$ and (b) temporal periods $\tau \leq 8$ on the parameter (P_c, K)-plane, with $P_c \in \{1, 2, ..., \frac{N}{2} - 1\}$ and $K \in [0.01, 5]$ for 100 equidistant values. Each pixel color is decided by the mode of 20 trajectories. The green curve is obtained from linear stability analysis of the zero synchronized state and the green dots are the corresponding wavenumber changes. The red dots mark the instability of the temporal period-2 states, obtained by numerical bifurcation analysis. Other parameters: $\gamma = 0.8$, $K_0 = 2$, $N = 100$, and random initial conditions $(p_j(0), \theta_j(0)) \in \mathrm{Uni}[-35, 35] \times \mathrm{Uni}[0, 2\pi)$, $j = 1, 2, ..., N$. Larger-size systems show similar phase transitions, cf. Appendix B.

furcation of the zero homogeneous states explained in Sec.III A; as P_c decreases, coherent patterns exhibit increasing wavenumbers l over progressively narrower sub-intervals of P_c; l appears independent of K, resulting in vertical strips rather than tongue-shaped regions as shown in [11, 21]. We refer to this layer as the *coherent region*;

- layer-V ($K \gtrsim 3.0$): chaotic motion dominates where the temporal period is large and the wavenumber appears random. This transition from a stable low-period state direct into chaos is observed in the locally coupled case [14], as well as in other systems [23–25].

The critical transitions in the diagrams can be explained by stability changes of the typical states: the green curve obtained from Eq.(2) marks the period-doubling bifurcations of the zero homogeneous states, with the green dots in Fig.3(a) indicating the wavenumber change, also predicted by Eq.(2). The boundary of chaos is given by the loss of stability of the temporal period-2 states, see the red curve [1] obtained by numerical bifurcation analysis implemented in BifurcationKit.jl in Julia [26]. Both curves agree excellently with the transitions observed in simulations.

Compared to the diagrams in Appendix A and in [11], first, there is no blowout bifurcation to full synchronization in the region of large coupling length P_c and large coupling strength K; second, there is no tongue-shaped region with a period-doubling cascade.

We emphasize that the diagrams show statistical behavior that only the most probable patterns are marked. In the coherent region (Layer-IV), states with different wavenumbers l coexist especially near the boundaries between adjacent l values. This can be characterized by the *relative basin size*, defined as the probability of reaching an attractor from a random initial condition. It is commonly used in many-body systems [27, 28] where the basins of attraction lie on a high-dimensional subspace in a highly nonlinear manner.

As observed in the coherent region (Layer-IV) in Fig.3, the wavenumber l is independent of the coupling strength

[1] Since the parameter P_c is discrete, the numerical continuation method does not apply here. Instead, we obtain the bifurcation points (P_c, K) discretely and interpolate the curve.

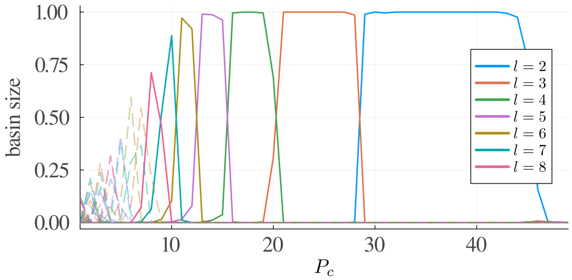

FIG. 4. Relative basin sizes for temporal period-2 states with wavenumbers l as a function of the coupling strength P_c. The dashed lines denote $l > 8$. Other parameters: $\gamma = 0.8$, $K_0 = 2$, $K = 1.5$, and $N = 100$.

K, so we fix $K = 1.5$ in this region. We simulate from a large number of random initial conditions [2] and compute the relative basin sizes as P_c varies. In Fig.4, smaller wavenumbers showing in the legend correspond to those in the coherent region in the phase diagram Fig.3(a); larger wavenumbers are dominant for smaller P_c and are shown in dashed curves. As observed, for $P_c \geq 10$, a single wavenumber tends to dominate and can act as the unique attractor, with its relative basin size reaching 1. In contrast, for smaller P_c, multiple wavenumbers l have comparable basin sizes and coexist simultaneously.

IV. SUPER-LONG TRANSIENT INTERFACE DYNAMICS

We have seen in the previous section rich dynamical patterns in the coupled dissipative kicked rotors where the local map is non-chaotic, yet chaos can emerge when the coupling strength K is large enough.

In this section, we examine the reverse scenario: when the local map is chaotic, the coupled system can still generate partially non-chaotic patterns, and depending on the coupling length P_c, these patterns can persist for an exponentially long time. With a large system size, transients become physically irrelevant and a fully chaotic state can never be achieved practically [29].

It has been shown that for large K_0, the single rotor system has coexisting regular and chaotic attractors [14]. We now consider initially a chain of N uncoupled rotors consisting of half-chain of chaotic rotors and the other half regular. It creates a domain wall between the two middle rotors $j = \frac{N}{2}, \frac{N}{2} + 1$, and the wall is stationary. Upon coupling, the domain wall becomes an interface, chaotic and regular motions can penetrate each other. Due to their relative basin sizes at the single-rotor level, the chaotic domain gradually encroaches the regular domain and eventually all rotors are chaotic. This has been observed in other coupled systems and has important implications in fluid dynamics [30].

Our interesting observation is that, depending on the parameter values (P_c, K), there is a sharp transition in the transient time before the system reaches a fully chaotic state.

To illustrate this phenomenon, we choose $K_0 = 6.6$ so that the single rotor has coexistence of a regular and a chaotic attractor, whose basin is shown in gray and yellow respectively in Fig.5(a). For simplicity, initial points are prepared such that rotors $j = 1, 2, ..., \frac{N}{2}$ are chosen randomly in a line segment I_0 inside the regular basin, and rotors $j = \frac{N}{2} + 1, ..., N$ are chosen in its counterpart, I_1, in the chaotic basin (this particular choice does not influence the dynamics since the chaotic basin is mixing).

Fig.5(b) shows the averaged transient time for a system of $N = 1000$ rotors with different values of (P_c, K). The iteration time $t = 1000$ is sufficient to detect the transition, i.e., the boundary separating long (dark-red) and short transient (light-yellow) regimes. The averaged transient time at $K = 1$ is illustrated in Fig.5(c): it increases exponentially with P_c until the transition occurs.

Fig.6 illustrates spatiotemporal evolutions of the $N = 1000$ system for $P_c = 10, 100$ and 300, showing three different regimes of the transient behavior: when the coupling length P_c is very small (Fig.6(a)), each rotor experiences localized interactions, and the domain wall propagates at a fixed speed in space, giving a short and predictable transient time. As P_c increases, the interactions become less local and a competition between chaos (as forcing or reaction) and coupling (as diffusion) emerges. In this regime, most regular rotors sustain themselves for an exponentially long time, see Fig.6(b). For very large P_c, the interactions are almost global, and the system effectively experiences a mean-field-like force, causing all rotors to rapidly “synchronize” to chaotic motions. In this case, the partially non-chaotic state survives for only $8 \sim 10$ iterations (Fig.6(c)). However, identifying precisely this transition curve is nontrivial and remains an open question for future work.

V. CONCLUSION

In this paper, we studied dynamics of a system of nonlocally coupled dissipative kicked rotors under variations of the coupling strength and the coupling length. We first analyzed the transition from a stationary homogeneous state to a coherent state of temporal period-2 via a period-doubling bifurcation. The spatial periodicity of coherent states are characterized by a wavenumber. As the coupling length decreases, the dominant wavenumber increases, which is also shown in the change of basin sizes. However, it is independent of the coupling strength in a certain range. These behaviors are summarized in the

[2] Note that since the whole phase space of the coupled system is a product of infinite cylinders, $M := ((-\infty, +\infty) \times [0, 2\pi))^N$, in practice we restrict to a subspace, namely, $([-p_0, p_0] \times [0, 2\pi))^N$ with $p_0 = 35$, so the basin sizes are conditioned on this subspace, where all the coherent states considered here are in this subspace.

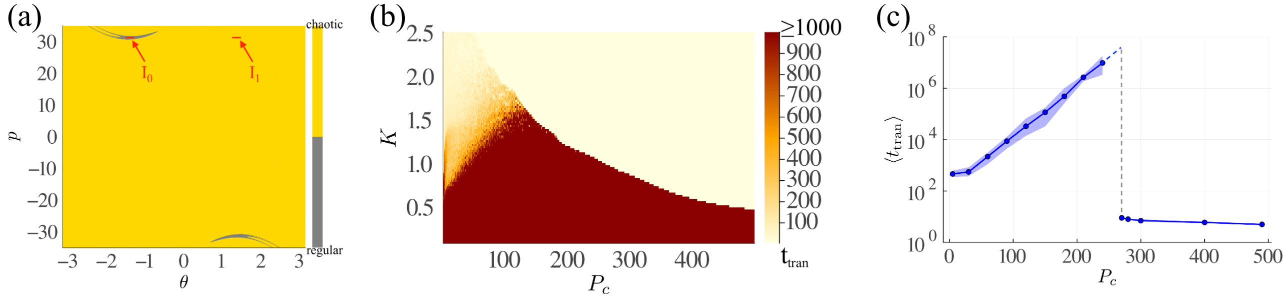

FIG. 5. Transient behavior for an $N = 1000$ system: (a) basin structure of the single rotor at $\gamma = 0.8$ and $K_0 = 6.6$, the two sub-intervals are $I_0 := [\theta^* - 0.05, \theta^* + 0.05]$ with $p_j(0) = p^*$, where $(p^*, \theta^*) = (10\pi, \arcsin \frac{-(1-\gamma)p^*}{K_0})$ is the fixed point of the single-rotor model and $I_1 := [-\theta^* - 0.05, -\theta^* + 0.05]$; I_0 (I_1) is a subset of the basin the regular (chaotic) attractor; (b) averaged transient time on the parameter (P_c, K)-plane and (c) for $K = 1$ in a semi-log scale: simulation data are shown in blue dots with fluctuations in blue ribbons; the gray dashed line marks the sharp transition.

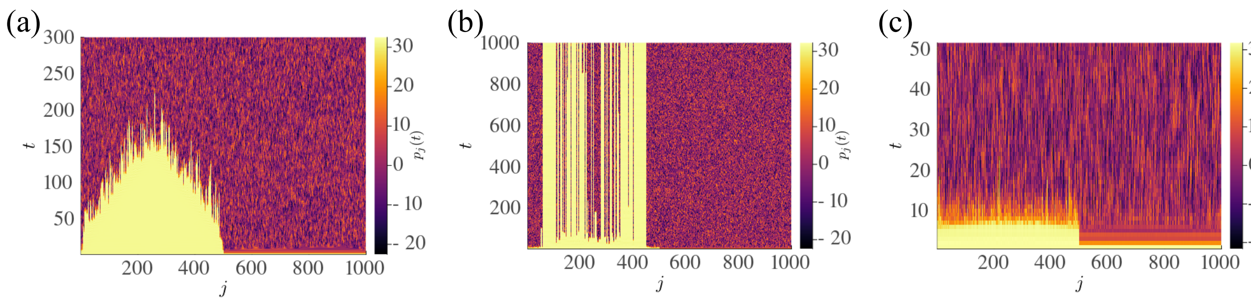

FIG. 6. Spatiotemporal evolutions of the rotor momenta $p_j(t)$ for $K = 1$: (a) a short transient at $P_c = 10$, (b) a long transient at $P_c = 100$, and (c) a very short transient at $P_c = 300$. Other parameters are the same as in Fig.5(b).

parameter space in Fig.3, where the region of coherent states, consisting of a sequence of reducing-sized strips labeling an increasing wavenumber, is bounded by the stability curves of the temporal period-2 states.

In the last section, we explored numerically a super-long transient phenomenon when the single rotor has co-existence of regular and chaotic attractors. At intermediate coupling lengths, the lifetime of a partially regular and partially chaotic state grows exponentially. Beyond a critical point, the transient time abruptly collapses to just a few iterations, and the system rapidly transitions to full chaos.

Many interesting questions remain open. For example, we did not discuss the transitions among the Layer-I and -II, Layer-III and -IV in Fig.3(b) as they are not the main focus of this paper, but it would be interesting to study them in detail. Second, the instability of the temporal period-2 states – marking the onset of chaos without developing a period-doubling (or multiplying) cascade – reveals a fundamental difference from the behavior in [11] (or in Appendix A). If we compare the local map, the single rotor exhibits a period-doubling cascade to chaos [13], but the cascade occurs almost immediately and does not follow the Feigenbaum universality [14]; while the logistic map (or Chebyshev maps in Appendix A) follows the Feigenbaum universality. This may explain the difference. But the question remains: are both phase diagrams generic, and under what conditions? Moreover, while we have illustrated the relative basin sizes of the different wavenumber states, the geometry of their basins of attraction changes in the phase space remains unclear. For the super-long transient interface phenomenon, one could explore alternative initial cluster configurations, for example, setting half-chain at one fixed point and the other half at the other fixed point. Given the dominance of the chaotic basin, such configurations will eventually reach fully chaotic states, but the interface would evolve differently than presented here. Finally, we leave the analytical prediction of the sharp lifetime transition for future work.

Appendix A: Coherent regions for coupled Chebyshev maps

The nth-order ($n \geq 2$) Chebyshev maps [31] are defined via $T_n(x) = \cos(n \arccos(x))$, $x \in [-1, 1]$, which can be written as polynomials, for example, $T_2(x) = 2x^2 - 1$, $T_3(x) = 4x^3 - 3x$, $T_4(x) = 8x^4 - 8x^2 + 1$, and so on. The 2nd-order Chebyshev map is equivalent to the logistic map, except that it is upside-down and defined on the interval

$[-1, 1]$. Therefore, the dynamics of the coupled T_2 system is expected to resemble that of the coupled chaotic logistic map [21], as confirmed in the first row of Fig.7. For higher orders n, the phase diagrams show similar patterns but the sizes of the tongue regions vary; see the last two rows in Fig.7 for $n = 3, 4$. In each left panel, the yellow region indicates a fully synchronized state, where the temporal dynamics follows the single Chebyshev map, which is chaotic.

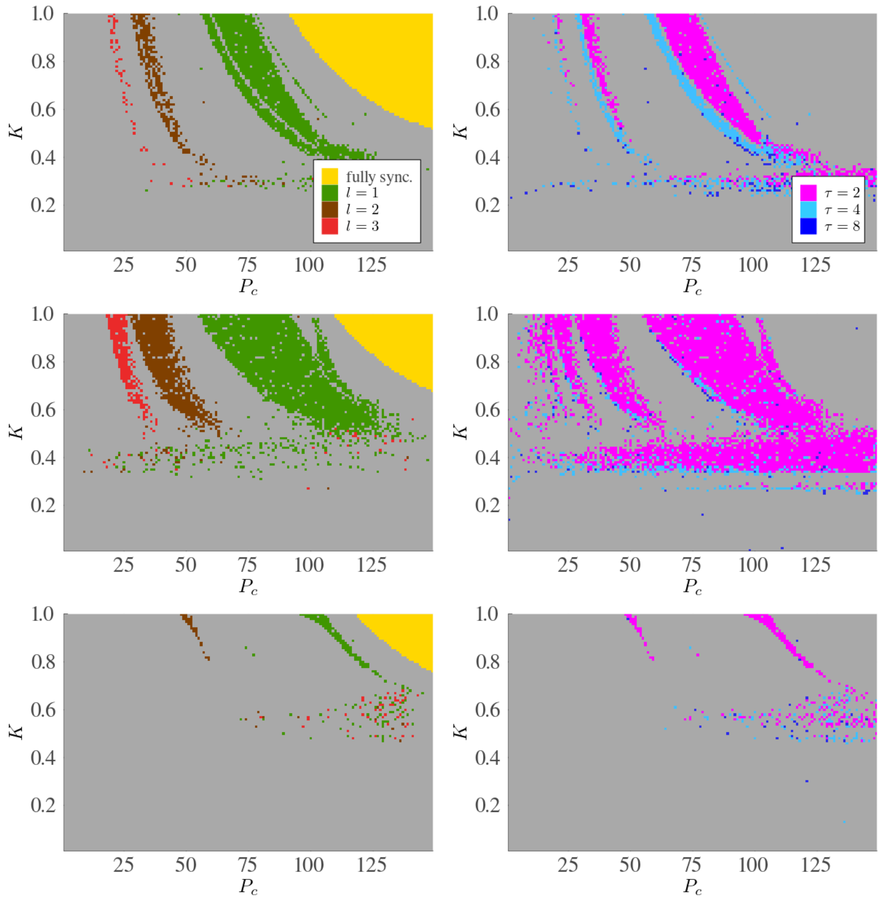

FIG. 7. Coherent regions for the system of nonlocally coupled Chebyshev maps T_n: T_2 (row 1), T_3 (row 2) and T_4 (row 3). The coupling scheme is the same as in Eq.(1). The left column shows wavenumbers $l = 1, 2, 3$ with temporal period $\tau \leq 8$ in green, brown and red, respectively, and the fully synchronized region in yellow; the right column shows temporal periods $\tau = 2, 4, 8$ in magenta, light blue and deep blue, respectively. All other patterns are colored in gray. Numerical settings: system size $N = 300$, $P_c \times K \in [1, 149] \times [0.01, 1]$ of resolution 149×100.

Appendix B: Coherent regions for coupled kicked rotors of larger system sizes

The coherent regions shown in Fig.3 are system-size independent. The plots below shows phase diagrams for $N = 300$ and 1000 systems. The diagram for the temporal period τ appears less layered when N is large, due to an increasing number of exceptional rotors in the system. The overall pattern still follows the temporal periodicity 2 in the coherent region.

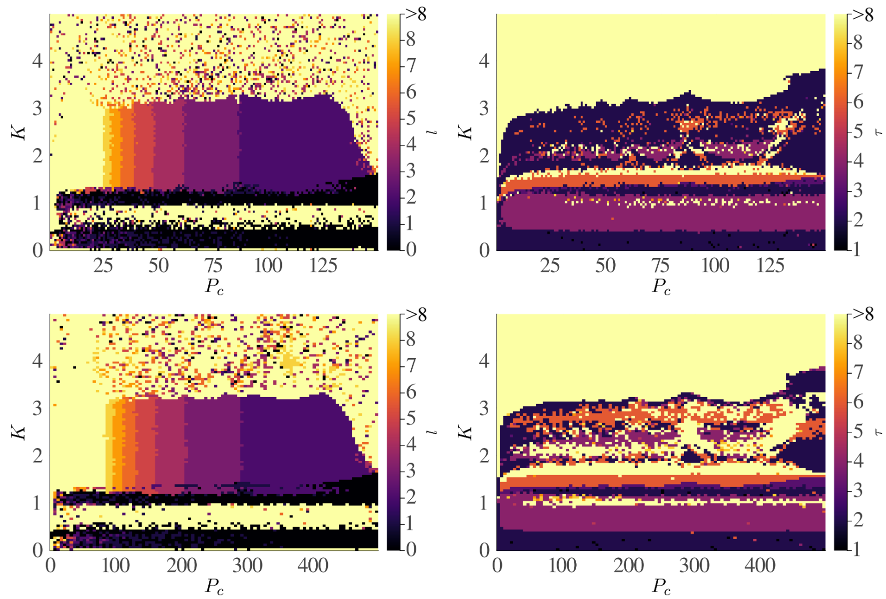

FIG. 8. Regions of typical wave numbers l and temporal periods τ in the parameter (P_c, K)-plane for the system sizes $N = 300$ (row 1) and 1000 (row 2). $P_c \in \{1, ..., \frac{N}{2} - 1\}$ and $K \in [0.01, 5]$ for 100 equidistant values. Each pixel color is decided by the mode of 10 trajectories. Other parameter values are as in Fig.3.

[1] Arkady Pikovsky, Michael Rosenblum, and Jürgen Kurths. *Synchronization: A universal concept in nonlinear sciences*. Cambridge University Press, Princeton, 2001.

[2] Pedro Fernando Almeida Di Donato, Elbert EN Macau, and Celso Grebogi. Phase locking control in the circle map. *Nonlinear Dynamics*, 47:75–82, 2007.

[3] Murray Shanahan. Metastable chimera states in community-structured oscillator networks. *Chaos: An Interdisciplinary Journal of Nonlinear Science*, 20(1), 2010.

[4] Emmanuelle Tognoli and JA Scott Kelso. The metastable brain. *Neuron*, 81(1):35–48, 2014.

[5] Louis M Pecora, Francesco Sorrentino, Aaron M Hagerstrom, Thomas E Murphy, and Rajarshi Roy. Cluster synchronization and isolated desynchronization in complex networks with symmetries. *Nature communications*, 5(1):4079, 2014.

[6] Daniel M Abrams and Steven H Strogatz. Chimera states for coupled oscillators. *Physical review letters*, 93(17):174102, 2004.

[7] Joseph D Hart, Kanika Bansal, Thomas E Murphy, and Rajarshi Roy. Experimental observation of chimera and cluster states in a minimal globally coupled network. *Chaos: an interdisciplinary journal of nonlinear science*, 26(9), 2016.

[8] Mark J Panaggio and Daniel M Abrams. Chimera states: coexistence of coherence and incoherence in networks of coupled oscillators. *Nonlinearity*, 28(3):R67, 2015.

[9] Eckehard Schöll. Synchronization patterns and chimera states in complex networks: Interplay of topology and dynamics. *The European Physical Journal Special Topics*, 225:891–919, 2016.

[10] Ralf Tönjes, Naoki Masuda, and Hiroshi Kori. Synchronization transition of identical phase oscillators in a directed small-world network. *Chaos: An Interdisciplinary Journal of Nonlinear Science*, 20(3), 2010.

[11] Iryna Omelchenko, Yuri Maistrenko, Philipp Hövel, and Eckehard Schöll. Loss of coherence in dynamical networks: spatial chaos and chimera states. *Physical review letters*, 106(23):234102, 2011.

[12] George M Zaslavsky. The simplest case of a strange attractor. *Physics Letters A*, 69(3):145–147, 1978.

[13] Angelo Russomanno. Spatiotemporally ordered patterns in a chain of coupled dissipative kicked rotors. *Physical Review B*, 108(9):094305, 2023.

[14] Jin Yan. Bifurcations and intermittency in coupled dissipative kicked rotors. *arXiv preprint arXiv:2503.13331*, 2025.

[15] Jörn Davidsen, Yuri Maistrenko, and Kenneth Showalter. Introduction to focus issue: Chimera states: From theory and experiments to technology and living systems. *Chaos: An Interdisciplinary Journal of Nonlinear Science*, 34(12), 2024.

[16] Mária Ercsey-Ravasz and Zoltán Toroczkai. Optimization hardness as transient chaos in an analog approach to constraint satisfaction. *Nature Physics*, 7(12):966–970, 2011.

[17] Stefanos Boccaletti, Celso Grebogi, Y-C Lai, Hector Mancini, and Diego Maza. The control of chaos: theory and applications. *Physics reports*, 329(3):103–197, 2000.

[18] Eckehard Schöll and Heinz Georg Schuster. Handbook of chaos control. 2008.

[19] Rubén Capeáns, Juan Sabuco, Miguel AF Sanjuán, and James A Yorke. Partially controlling transient chaos in the lorenz equations. *Philosophical Transactions of the Royal Society A: Mathematical, Physical and Engineering Sciences*, 375(2088):20160211, 2017.

[20] Guanglei Wang, Ying-Cheng Lai, and Celso Grebogi. Transient chaos-a resolution of breakdown of quantum-classical correspondence in optomechanics. *Scientific reports*, 6(1):35381, 2016.

[21] Iryna Omelchenko, Bruno Riemenschneider, Philipp Hövel, Yuri Maistrenko, and Eckehard Schöll. Transition from spatial coherence to incoherence in coupled chaotic systems. *Physical Review E—Statistical, Nonlinear, and Soft Matter Physics*, 85(2):026212, 2012.

[22] Anna Zakharova, Marie Kapeller, and Eckehard Schöll. Amplitude chimeras and chimera death in dynamical networks. In *Journal of Physics: Conference Series*, volume 727, page 012018. IOP Publishing, 2016.

[23] Takeshi Kawabe and Yoshiro Kondo. Intermittent chaos generated by logarithmic map. *Progress of theoretical physics*, 86(3):581–586, 1991.

[24] Christian Beck, Ugur Tirnakli, and Constantino Tsallis. Generalization of the gauss map: A jump into chaos with universal features. *Physical Review E*, 110(6):064213, 2024.

[25] Charles H Bennett, G Grinstein, Yu He, C Jayaprakash, and David Mukamel. Stability of temporally periodic states of classical many-body systems. *Physical Review A*, 41(4):1932, 1990.

[26] Romain Veltz. BifurcationKit.jl, July 2020.

[27] Daniel A Wiley, Steven H Strogatz, and Michelle Girvan. The size of the sync basin. *Chaos: An Interdisciplinary Journal of Nonlinear Science*, 16(1), 2006.

[28] Yuanzhao Zhang, Per Sebastian Skardal, Federico Battiston, Giovanni Petri, and Maxime Lucas. Deeper but smaller: Higher-order interactions increase linear stability but shrink basins. *Science Advances*, 10(40):eado8049, 2024.

[29] James P Crutchfield and Kunihiko Kaneko. Are attractors relevant to turbulence? *Physical review letters*, 60(26):2715, 1988.

[30] James D Keeler and J Doyne Farmer. Robust space-time intermittency and 1f noise. *Physica D: Nonlinear Phenomena*, 23(1-3):413–435, 1986.

[31] Jin Yan and Christian Beck. Distinguished correlation properties of chebyshev dynamical systems and their generalisations. *Chaos, Solitons & Fractals: X*, 5:100035, 2020.